Numerical study of disperse materials process in a continuous-flow plasma reactor

Issakhov A.A., Urmashev B.A.

***Abstract*—** the paper presents a numerical study of the temperature propagation in the direct-flow plasma reactor, which is solved by the compressible Navier - Stokes equations that is approximated by finite volume method, the numerical algorithm based on the SIMPLE method. In the numerical algorithm of the equation system can be divided into four stages. The first stage is that the transfer of momentum carried out only by convection and diffusion. The intermediate velocity field is solved by the solution of the differential velocity gradient equation with the Green-Gauss Cell Based scheme. For the pressure field is applied PRESTO numerical scheme. In a third step it is assumed that the transfer is carried out only by the pressure gradient. The fourth step of the equation is solved for the energy transport equation as well as the momentum equations by the Green-Gauss Cell Based scheme. The algorithm is parallelized on high-performance systems. With this numerical algorithm was obtained numerical results of temperature distribution in a continuous-flow plasma reactor. Numerical modelling allows us to give a more precise description of the processes that have been identified and studied theoretically and can reveal new physical phenomena processes that are not yet available, seen in experimental studies. Simulation results show that the constructed numerical model provides the necessary accuracy and stability, which should accurately describe the process during the time interval.

***Keywords*—** direct flow plasma reactor, numerical simulation, Navier-Stokes equations, finite volume method, the SIMPLE algorithm.

I. Introduction

IN modern industry, construction and protective materials receive wide and effective use of some powders consisting of hollow microparticles (hollow powder's). Hollow ceramic powders used in the manufacture of composite heat and acoustic insulation materials, light construction and cement fillers, buoyancy elements, explosive mixtures, as well as provide a basis for catalysts pit, adsorbents, filter elements, encapsulating medium and etc. Getting hollow microspheres with a given chemical composition and mechanical properties substantially expand the circle of solved problems in the construction and protective materials industry.

The relevance of the problem of getting dispersed materials undoubtedly due to their highly diverse applications in industry. Toughness is the most of their valuable property. One of the main applications of highly dispersed materials in the industrial production is to use them as an intermediate phase at producing materials with a high degree activity. In due time the aerosol dispersed materials technology has played a decisive role in ensuring of increasing of uranium – 235, production of nuclear fuel. The natural uranium of this isotope it is very small only about 0.7%. To highlight this precious isotope, uranium is converted into the gaseous compound - the uranium hexafluoride. This compound is then repeatedly passed through a diffusion baffle, a kind of sieve. The compound lighter uranium - 235 is diffused slightly faster than uranium hexafluoride 238 - only 1,005 times. But this is tiny advantage can be realized only when the pore baffle size is much less than the free path length of the UF6 molecules, which is the order of 10^{-8} m. Producing of such partition is possible only by pressing and sintering particles having a size of the same order.

Historically, the first dispersed product is soot, which was obtained by spray. There are three types of soot: canal, thermal and heating. Canal soot obtained by incomplete natural gas combustion in a rectangular cross section channel, with walls, which then collected it. Thermal soot obtained not by combustion, but by the natural gas decomposition by passing it through the heated outside the channel. This method gives the largest soot particles up to 10^{-8} m radius. The largest capacity provides an oven method in which in a special chamber undergoes incomplete atomized liquid mixture combustion of hydrocarbons. The resulting aerosol is cooled by passing through a special tower and enters into the apparatus for soot deposition. Soot particles represent balls with the size of 10^{-9} — 10^{-8} m aggregated into flakes up to 10^{-6} m, containing thousands of "primary" balls. Soot is used not only as filler but also as a black pigment [2].

Dispersed systems - the heterogeneous systems of two or more phases with a high surface area between them. Typically, one of the phases forms a continuous dispersion medium, which is distributed in the volume dispersed phase (dispersed phase or more) as small crystals, solid amorphous particles, droplets or air bubbles. Dispersed systems may have more complex structure, for example, be a two-phase formation, which each phases being continuous, enters the other phase volume. Such systems include solids, filled with an extensive system of channels-pores, filled with gas or liquid, some microheterogenous polymer compositions and others. There are cases when the dispersion medium "degenerates" to the

This work is supported by the grant from the Ministry of education and science of the Republic of Kazakhstan.

A. Issakhov al-Farabi Kazakh National University, 050040, Almaty, Kazakhstan (e-mail: alibek.issakhov@gmail.com)

B.A. Urmashev al-Farabi Kazakh National University, 050040, Almaty, Kazakhstan (baidaulet.urmashev@kaznu.kz)

subtlest layers (membranes), separating the particles of the dispersed phase [1].

II. FORMATION OF HOLLOW SPHERE

When processing powder materials for example ZrO2, SiO2, Ni, CoNiCrAlY in a plasma jet: the basic condition for the formation of hollow particles is sufficient content of the gas phase of the initial powder. Now a day, a large number of methods of plasma processing known for the hollow spheres preparation of different chemical composition and size. This can be achieved by several methods: microporous particles prior sorption of gases, gas emission due to thermal decomposition or chemical reaction. One of the most effective methods of producing hollow particles - plasma treatment of the agglomerated powders. The possibility of obtaining hollow particle tens of microns diameter and thickness of the nanosized shell experimentally tested for plasma processing to submicron powder for example SiO2, with a mean particle size of 110 nm [16, 17].

Consider a simple scenario of forming a hollow sphere of porous particles with a diameter D_p and open porosity p, which is being uniformly independent. When a porous agglomerate enters to the plasma jet of its material, the inner gas is heated (Figure 1). While it leaves the gas expands the volume of particles, but the pore volume remains unchanged. At a time when the surface of the particles reaches the liquid melting temperature is formed by the shell. It captures and fixes the mass of gas inside the particle. The trapped gas collects into a single central cavity, which depends on temperature and ambient pressure the size. The particles of the starting powder of silicon dioxide (SiO2) (Figure 2) are agglomerates with a diameter $D_p = 50-150$ *microns* comprised of cemented grain size of 3-5 microns. Separate agglomerate contains about 10^3-10^5 grains, average volume porosity of initial powder is about 50%. In Figure 3 it can be seen that the particles of silicon dioxide (SiO2) powder, subjected to processing in the plasma flow, optically transparent, have a smooth surface without holes is a single gas inside the cavity; particles retain the original diameter of 50-150 microns, or crushed to a size up to 5 microns coating thickness D_p equal to 10-20% of the particle diameter D_p. The ratio of gas mass to the mass of the particles in the raw agglomerates is at the level of SiO2 $m_g / m_p = 2*10^{-4}$ and melting the material at a temperature (T=3000K) $m_g / m_p = 2*10^{-5}$ [16, 17].

In order to study the features of the production of hollow microspheres of SiO2 powder experiments on the use of linear circuits of the plasma torch with radial powder injection were carried out under the section of the nozzle at a distance of 25 mm.

When the power characteristics of the plasma torch (nitrogen plasma), thermal power $P_T = 3{,}7\,\text{kW}$, the average size of the obtained hollow particles are 20 microns.

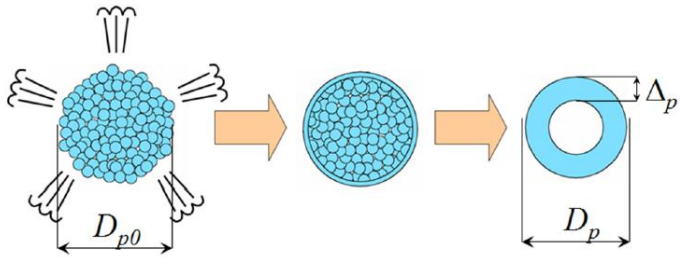

Figure 1 - Scenario of hollow spheres formation of a porous agglomerates

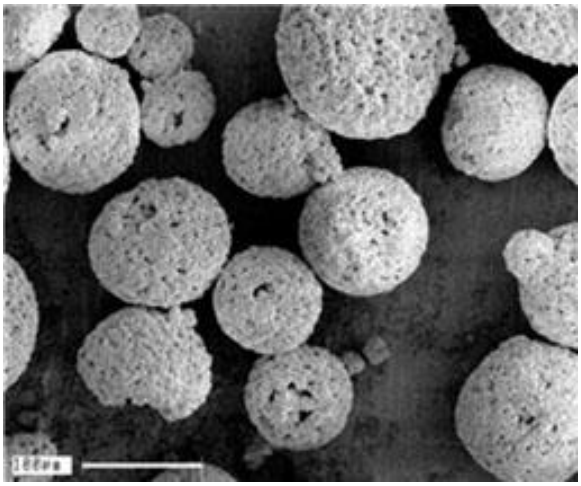

Figure 2 - The typical form of powder - SiO2 agglomerates

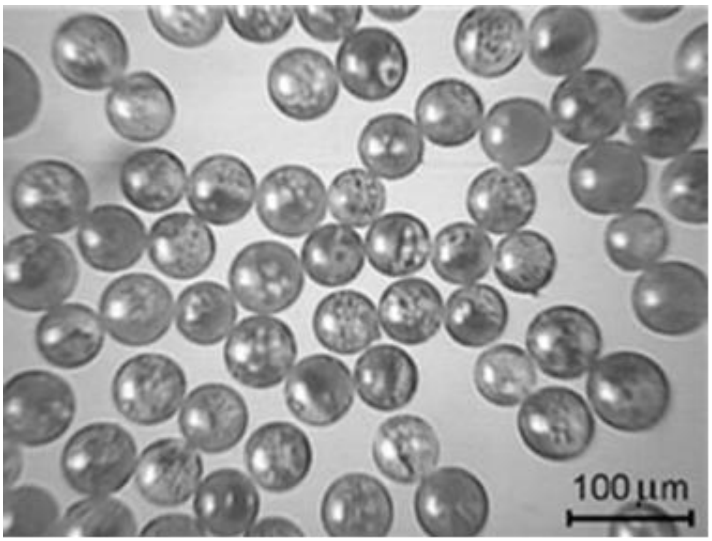

Figure 3 - Hollow microspheres last treatment in the plasma jet (optical microscope photograph)

III. MATHEMATICAL MODEL

In discrete analogues of the transport coefficients on the faces of control volumes are determined by harmonically average value, to allow for intermittent changes in the properties of the medium and to achieve enough correct conjugation at the phase boundary. In solids used the thermophysical properties of the wall material (electrode) with the temperature determining of the heavy particles. To account

the heating of the wall by volumetric radiation is assumed that the radiation energy is absorbed by the surface layer of the control volumes wall and considered there as a local source of heat. Then this energy is given by conduction deeply into the wall and back – to the gas which is adjacent to the wall. To satisfy the safety of wall there is placed a limit on the calculated temperature that does not exceed the melting point of the wall material. Such approach allows us to consider both thermal processes in solids, plasma and gas, and to apply a uniform method of solving equations in the whole computational domain. In the paper [3] developed a method for simulation the characteristics of the arc from the "cathode to anode" and got a satisfactory agreement with the experimental results of the simulation. This method is convenient to use and does not require any additional information to define the boundary conditions near the solids and relatively easy allows taking into account the form and material of electrodes. The size and location of the cathode and anode arc bindings, the distribution of current density and temperature in the electrodes and the plasma set in the numerical solution as a result of the self-consistent interaction of the thermal, electromagnetic and gas-dynamic characteristics.

In accordance with this, while simulating the atmospheric pressure of the high-current arc, it is possible did not penetrate into the complex kinetics near electrode processes in the first approximation and for crosslinking solutions, obtained in the electrodes and the plasma, to carry out a simplified scheme: the electrode-plasma.

Now it is known many mathematical models which describe the interaction of electric arc and gas flow in the plasmatron [4-9]. Investigation of the plasmtron's arc propagation with complex geometry is relevant for determining the turbulence and nonequilibrium phenomena formation in the generation of the plasma flow.

For the development of a numerical model was considered the following assumptions:

- The particles are moving in one direction about the axis of the plasma stream,
- Uniformity of temperature is performed by the particle volume,
- Takes into account the radiational heat consumption,
- Radiation transfer neglect from the plasma to a particle,
- There are no evaporation particles.

In the considered thermal problem for the hollow particles the characteristic size of the particle is the wall thickness δ. From the considered assumptions, depending on the radius of the particles, it was found that the radiation heat consumption in the heat exchange with the gas is only 5%.

The mathematical model is based on Reynolds-Averaged Navier-Stokes equations. The Boussinesq approximation is applied to leads to the following system of equations, where for turbulence modelling is chosen the $k-\varepsilon$ model [10-15]:

$$\frac{\partial \rho}{\partial t}+\frac{\partial \rho u_j}{\partial x_j}=0 \quad (1)$$

$$\frac{\partial \rho u_i}{\partial t}+\frac{\partial}{\partial x_j}(\rho u_i u_j)=-\frac{\partial p'}{\partial x_i}+\frac{\partial}{\partial x_j}\left[\mu_{eff}\left(\frac{\partial u_i}{\partial x_j}+\frac{\partial u_j}{\partial x_i}\right)\right] \quad (2)$$

$$\frac{\partial E}{\partial t}+\frac{\partial}{\partial x_j}(u_j E)=\frac{\partial u_j E}{\partial x_j}+\frac{\partial q_j}{\partial x_j} \quad (3)$$

$$p=\rho RT \quad (4)$$

where u_j are the velocity components, E – total energy, x_j are the Cartesian coordinate directions, ρ is the mixture density, μ_t is the turbulent viscosity, μ is the viscosity, k is the turbulent kinetic energy, ε is the dissipation rate, μ_{eff} – effective viscosity, p' – modified pressure. Here $p'=p+\frac{2}{3}\rho k+\frac{2}{3}\mu_{eff}\frac{\partial u_k}{\partial x_k}$ and $\mu_{eff}=\mu+\mu_t$, where $\mu_t=C_\mu\rho\frac{k^2}{\varepsilon}$ – turbulence viscosity, $P_k=\mu_{eff}\left(\frac{\partial u_i}{\partial x_j}+\frac{\partial u_j}{\partial x_i}\right)-\frac{2}{3}\mu_{eff}\frac{\partial u_k}{\partial x_k}\delta_{ij}$, $q=-k\frac{\partial T}{\partial x_j}$, $E=\rho(e+\frac{u^2}{2})$, $e=c_v T$.

$$\frac{\partial k}{\partial t}+\frac{\partial}{\partial x_j}(u_j k)=\frac{\partial}{\partial x_j}\left[\left(\mu+\frac{\mu_t}{\sigma_k}\right)\frac{\partial k}{\partial x_j}\right]+P_k-\rho\varepsilon+P_{kb} \quad (5)$$

$$\frac{\partial \varepsilon}{\partial t}+\frac{\partial}{\partial x_j}(u_j\varepsilon)=\frac{\partial}{\partial x_j}\left[\left(\mu+\frac{\mu_t}{\sigma_\varepsilon}\right)\frac{\partial \varepsilon}{\partial x_j}\right]+\frac{\varepsilon}{k}(C_{\varepsilon 1}P_k-C_{\varepsilon 2}\rho\varepsilon+C_{\varepsilon 1}P_{\varepsilon b}) \quad (6)$$

P_k – turbulent production due to viscous forces, which is represented as:

$$P_k=\mu_t\left(\frac{\partial u_i}{\partial x_j}+\frac{\partial u_j}{\partial x_i}\right)\frac{\partial u_i}{\partial x_j}-\frac{2}{3}\frac{\partial u_k}{\partial x_k}\left(3\mu_t\frac{\partial u_k}{\partial x_k}+\rho k\right) \quad (7)$$

$P_{kb}, P_{\varepsilon b}$ –represent the buoyancy forces, where $P_{kb}=-\frac{\mu_t}{\rho\sigma_\rho}\rho\beta g_i\frac{\partial T}{\partial x_i}$ and $P_{\varepsilon b}=C_3\max(0,P_{kb})$. Here β is the coefficient of thermal expansion, $\sigma_\rho=0.9$, $C_{\varepsilon 1,}C_{\varepsilon 2}$, $\sigma_k,\sigma_\varepsilon$ – are constants. For the numerical solution was chosen the SIMPLE algorithm.

IV. NUMERICAL ALGORITHM

For the numerical simulation of the system of equation (1) – (7) is applied the SIMPLE (Semi-Implicit Method for Pressure Linked Equations) algorithm. This algorithm was first developed by B. Spalding and S. Patankar [18].

The SIMPLE algorithm implements like projection method [19-29]. The solution of the system of equation (1) – (7) using SIMPLE algorithm is described shortly with the following steps:

1. First, we set the boundary conditions.
2. The second step is a computation of velocity gradient. For the solution of the differential velocity gradient equation, the Green-Gauss Cell Based scheme is used.
3. After the second step, the pressure gradient is computed. For the pressure field, PRESTO numerical scheme is applied.
4. In order to calculate the intermediate velocity field the discretized momentum equation is solved via the Second Order Upwind scheme.
5. The fifth step is the computation of the uncorrected face mass fluxes.
6. Production of the pressure correction cell values is done at sixth step due to the solution of the pressure correction equation.
7. At the seventh step, we update the pressure field $p^{k+1} = p^k + urf \bullet p'$, where urf stands for the under-relaxation factor for pressure.
8. After updating the pressure field itself, we update the boundary pressure corrections p'_b.
9. At the ninth step we correct the face mass fluxes as following: $\dot{m}_f^{k+1} = \dot{m}_f^* + \dot{m}'_f$
10. Correction of the cell velocities is done via the solution of next equation: $\vec{v}^{k+1} = \vec{v}^* - \frac{Vol\nabla p'}{\vec{a}_P^v}$.
11. At the eleventh step, the Volume fraction equation is solved via the CICSAM scheme.
12. The turbulent kinetic energy is solved via the Second order upwind numerical scheme.
13. The thirteenth step is the solution of the Dissipation rate equation, which is done with the application of the Second order upwind scheme.
14. At last step, density and viscosity are updated due to pressure changes.

V. FORMULATION OF THE PROBLEM

Figure 4 shows a schematic representation of the plasmatron. This figure also indicates all dimensions of the plasmatron. To start simulations, initial and boundary conditions were given. Initial conditions for velocity, pressure, density and temperature are given in the following form: $u_j = 0, \quad (j = 1,2,3),\ T = 20^0 C, \rho = 1.25\ kg/m^3, P = 1\ atm.$ The boundary conditions for velocity, pressure, density and temperature are specified, as indicated in figure 5. Also, additional boundary conditions are set for the temperature, depending on the size and location of the heat source. At the lateral boundaries, the non-slip conditions are set for the velocity (Figure 5).

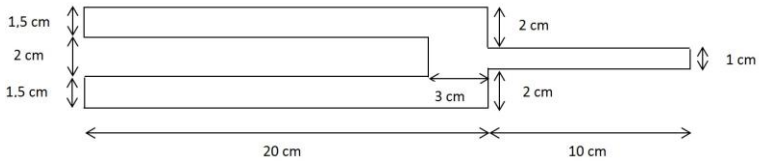

Figure 4 – Schematic view of plasmatron.

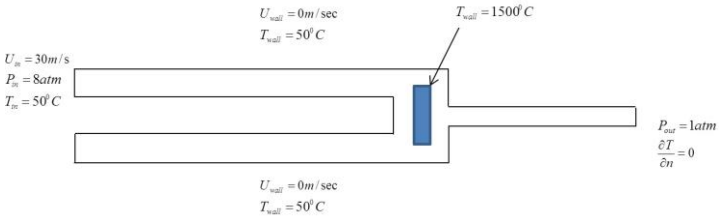

Figure 5 – Boundary conditions.

VI. NUMERICAL SIMULATION RESULTS

For the numerical simulation, the corresponding initial and boundary conditions were given. The simulations used a computational grid with more than 300,000 computational nodes. To study the temperature distribution, in a direct flow plasma reactor used the mathematical model, which based on Reynolds averaged Navier-Stokes (RANS) equations and the SIMPLE algorithm. Figure 6 shows the density distribution contour for different time layers in a direct-flow plasma reactor. And in Figure 7 is shown the contour of Mach number distribution for different time layers in a direct-flow plasma reactor. In Figure 8 it can be seen the velocity distribution contour for different time layers in a direct-flow plasma reactor. And in Figure 9 is shown the pressure distribution contour for different time layers in a direct-flow plasma reactor. Figure 10 shows the temperature distribution profile for different time layers in a direct-flow plasma reactor.

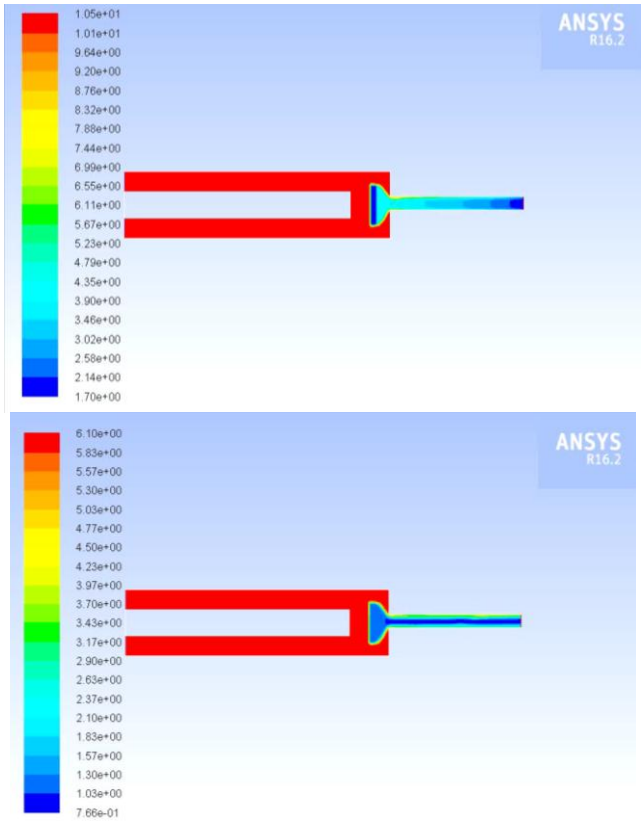

Figure 6 – The density distribution contour for different time layers ((a) t = 1 sec, (b) t = 15 sec, (c) t = 30 sec) in a direct-flow plasma reactor.

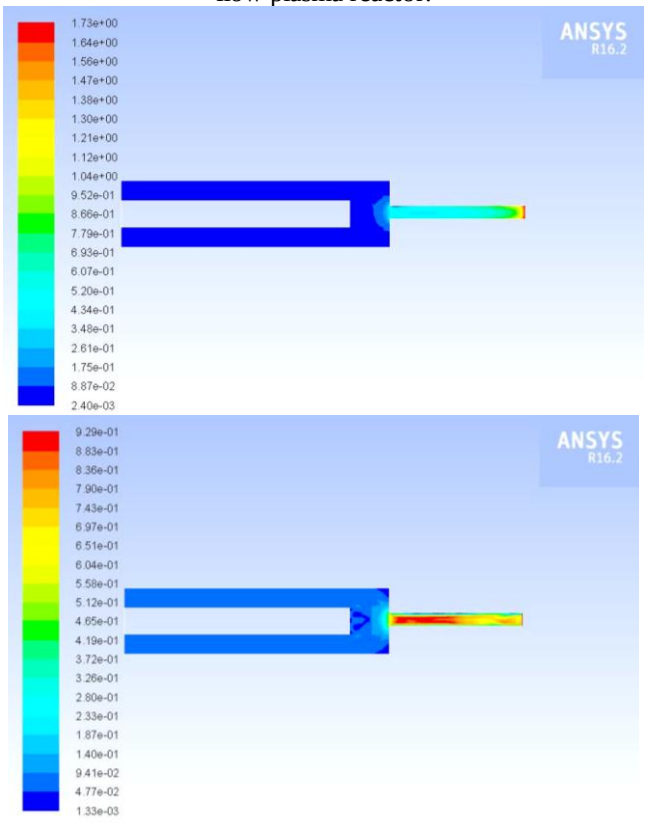

Figure 7 – The Mach number distribution contour for different time layers ((a) t = 1 sec, (b) t = 15 sec, (c) t = 30 sec) in a direct-flow plasma reactor.

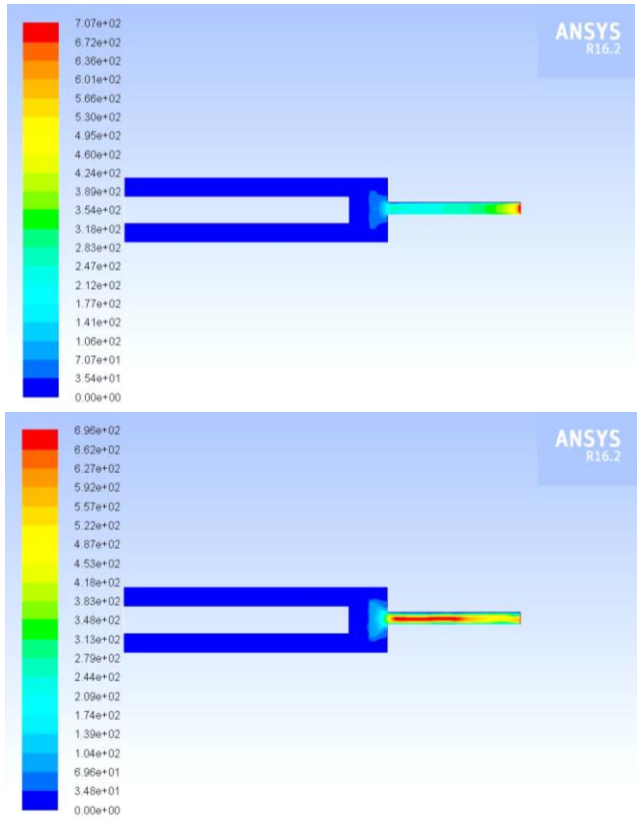

Figure 8 – The velosity distribution contour for different time layers ((a) t = 1 sec, (b) t = 15 sec, (c) t = 30 sec) in a direct-flow plasma reactor.

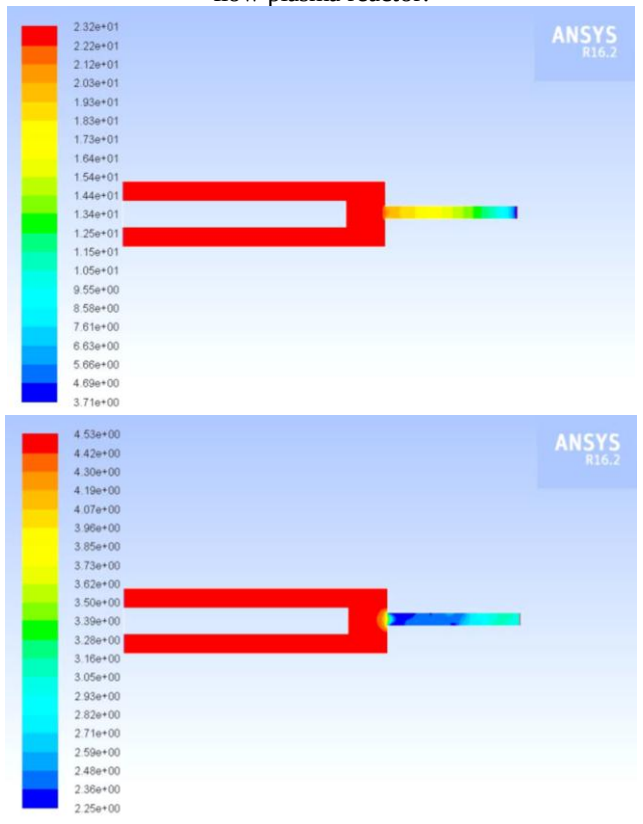

Figure 9 – The pressure distribution contour for different time layers ((a) t = 1 sec, (b) t = 15 sec, (c) t = 30 sec) in a direct-flow plasma reactor.

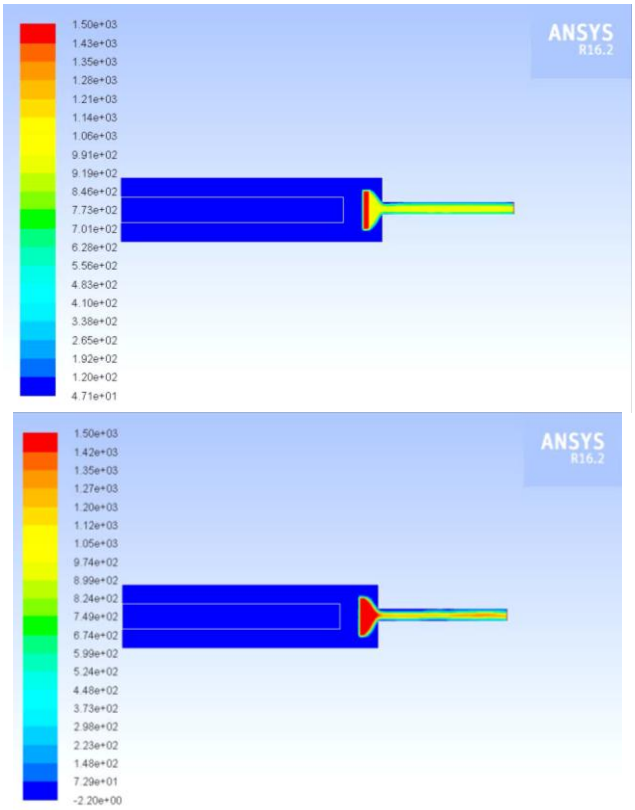

Figure 10 – The temperature distribution contour for different time layers ((a) t = 1 sec, (b) t = 15 sec, (c) t = 30 sec) in a direct-flow plasma reactor.

VII. Conclusions

In the work were carried out numerical modelling of the thermal processes distribution in the direct flow plasma reactor. This gave a deeper understanding of inner flow in direct flow plasma reactor. Numerical simulation can provide a more accurate description of the technical processes that have been identified or studied theoretically by the laboratory. And also show new physical phenomena processes, which not available to see in experimental studies yet.

In the simulation we consider the development of around jet in a coaxial flow of argon (Ar) at a rate of 29 -30 l/min., with the supplied 10-12 gr./min. of ash. For the modelling of a turbulent flow used compressible Navier-Stokes equations consisting of the continuity equation, the momentum equations, the energy equation and equation of state.

Simulation results show that the constructed numerical model provides the necessary accuracy and stability, which should accurately describe the process during the time interval. Here the solution is limited by time, space and the possible range of other physical parameters. It has been found that setting of the boundary conditions is an important task.

VIII. ACKNOWLEDGMENT

This work is supported by the grant from the Ministry of education and science of the Republic of Kazakhstan.

REFERENCES

[1]. Rabinovich V.A. Dispersnye sistemy. — Bol'shaja jenciklopedija himii, 1985. –704 p. (in Russian).
[2]. Ur'ev N. B. Vysokokoncentrirovannye dispersnye sistemy. – M., 1980. - 502 p. (in Russian).
[3]. Patankar S. Chiclennye metody peshenija zadach teploobmena i dinamiki zhidkocti. – M.: Jenepgoatomizdat, 1984. – 152 p. (in Russian).
[4]. Semenov B.F. Raschet tupbulentnogo potoka gaza v kanale plazmotrona so stupenchatym jelektpodom // – Vestnik Kypgyzcko-Poccijskogo Slavjanckogo univepsiteta. - 2003. № 5. (in Russian).
[5]. Jengel'sht B.S., Gupovich B.C., Decjatkov G.A. i dr. Teorija stolba jelektricheskoj dugi. -– Hovosibirsk: Hauka SO, 1990, V. 1, – 376 p. (in Russian).
[6]. Zhajnakov A., Urusov R.M., Urusova T.Je. Chislennyj analiz neosesimmetrichnyh jelektpicheskih dug. — Bishkek: Ilim, 2001. – 232 p. (in Russian).
[7]. Panevin I.G., Hvecjuk B.I., Hazarenko I.P. i dr. Teorija i raschet prijelektrodnyh processov. -– Hovosibirsk: Hauka SO, V. 10, 1992. – 197 p. (in Russian).
[8]. Zhukov M.F., Zacypkin I.M., Timoshevskij A.N. i dr. Jelektpodugovye generatory termicheskoj plazmy. -– Hovosibirsk: Hauka CP RAN, V. 17, 1999. – 712 p. (in Russian).
[9]. Zhukov M.F., Koroteev A.S., Urjukov B.A. Prikladnaja dinamika termicheskoj plazmy. -– Hovosibirsk: Hauka SO, 1975. – 298 p. (in Russian).
[10]. Wilcox D. C. Turbulence Modeling for CFD, 2nd ed. DCW Industries, 2006
[11]. Shih T. H., Liou W. W., Shabbir A., Yang Z., Zhu J. A New k-ε Eddy Viscosity Model for High Reynolds Number Turbulent Flows—Model Development and Validation. Computers & Fluids. 24(3):227-238, 1995
[12]. Chung T. J. Computational Fluid Dynamics. Cambridge University Press, 2002 – p. 1012.
[13]. Ferziger J. H., Peric M. Computational Methods for Fluid Dynamics. Springer; 3rd edition, 2013, p. 426.
[14]. Peyret R., Taylor D. Th. Computational Methods for Fluid Flow. New York: Berlin: Springer-Verlag. 1983, p. 358.
[15]. Roache P.J. Computational Fluid Dynamics, Albuquerque, NM: Hermosa Publications. 1972, p. 434.
[16]. Solonenko O.P., Gulyaev I.P., Smirnov A.V. Thermal plasma processes for production of hollow spherical powders: theory and experiment. Journal of Thermal Science and Technology 6 (2), 219-234, 2011.
[17]. Gulyaev I.P. Production and modification of hollow powders in plasma under controlled pressure. Journal of Physics: Conference Series 441 (1), 012033, 2013.
[18]. Patankar, S. V., Spalding, D.B. A calculation procedure for heat, mass and momentum transfer in three-dimensional parabolic flows, Int. J. of Heat and Mass Transfer, Volume 15, Issue 10, 1972, pp. 1787-1806.
[19]. Issakhov A. "Mathematical Modelling of Thermal Process to Aquatic Environment with Different Hydrometeorological Conditions". The Scientific World

Journal, vol. 2014, Article ID 678095, 10 pages, 2014. doi:10.1155/2014/678095

[20]. Issakhov A. "Modeling of Synthetic Turbulence Generation in Boundary Layer by Using Zonal RANS/LES Method". International Journal of Nonlinear Sciences and Numerical Simulation. Volume 15, Issue 2, Pages 115–120, DOI: 10.1515/ijnsns-2012-0029, 2014

[21]. Issakhov A. "Mathematical Modeling of the Discharged Heat Water Effect on the Aquatic Environment from Thermal Power Plant". International Journal of Nonlinear Sciences and Numerical Simulation. Volume 16, Issue 5, Pages 229–238, DOI: 10.1515/ijnsns-2015-0047, June 2015

[22]. Issakhov A. "Mathematical modeling of the discharged heat water effect on the aquatic environment from thermal power plant under various operational capacities". Applied Mathematical Modelling, Volume 40, Issue 2, 15 January 2016, Pages 1082–1096

[23]. Issakhov A. "Mathematical Modelling of the Thermal Process in the Aquatic Environment with Considering the Hydrometeorological Condition at the Reservoir-Cooler by Using Parallel Technologies". Sustaining Power Resources through Energy Optimization and Engineering, Editors: Vasant, Pandian, and Nikolai Voropai. IGI Global, 2016, pp. 1-494, doi:10.4018/978-1-4666-9755-3, Chapter 10, 2016, pp. 227-243, DOI: 10.4018/978-1-4666-9755-3.ch010

[24]. Issakhov A. "Numerical modelling of distribution the discharged heat water from thermal power plant on the aquatic environment". AIP Conference Proceedings 1738, 480025 (2016); doi: 10.1063/1.4952261.

[25]. Issakhov, A.; "Mathematical Modelling of the Influence of Thermal Power Plant on the Aquatic Environment with Different Meteorological Condition by Using Parallel Technologies". Power, Control and Optimization. Lecture Notes in Electrical Engineering. 239, 165–179 (2013).

[26]. Issakhov A. "Numerical modelling of the thermal effects on the aquatic environment from the thermal power plant by using two water discharge pipes". AIP Conference Proceedings 1863, 560050 (2017); doi: http://dx.doi.org/10.1063 /1.4992733

[27]. Issakhov, A.; "Mathematical modelling of the influence of thermal power plant to the aquatic environment by using parallel technologies". AIP Conf. Proc. 1499, 15–18, (2012), doi: http://dx.doi.org /10.1063/ 1.4768963

[28]. Issakhov, A.; "Numerical study of the discharged heat water effect on the aquatic environment from thermal power plant by using two water discharged pipes," International Journal of Nonlinear Sciences and Numerical Simulation. 18(6): 469-483, (2017). https://doi.org/10.1515/ijnsns-2016-0011.

[29]. Issakhov, A.; "Numerical modeling of the effect of discharged hot water on the aquatic environment from a thermal power plant". International Journal of Energy for a Clean Environment, Volume 16, Issue 1-4, 2015, pages 23-28, DOI: 10.1615/InterJEnerCleanEnv.2016015438